Batchamen Mougnol *et al.*
Environmental Systems Research (2022) 11:25
https://doi.org/10.1186/s40068-022-00271-7

Environmental Systems Research

RESEARCH

Open Access

Synthesis of eco-friendly ZnO-based heterophotocatalysts with enhanced properties under visible light in the degradation of organic pollutants

Jean Bedel Batchamen Mougnol[1*], Frans Waanders[1], Seteno Karabo Obed Ntwampe[1], Elvis Fosso-Kankeu[2] and Ali Rashed Al Alili[3]

Abstract

Heterogeneous photocatalysts have been widely used for the removal of various organic pollutants from wastewater. The main challenge so far resides in the sustainability of the process, with regard to the synthesis and the application under visible light. In this study the precipitated materials from the *Moringa oleifera* seed (MO), groundnut shells (GS) and apatite (A) agrowastes were functionalized with zinc oxide (ZnO) and silver (Ag) solution, to produce a novel bio-heterophotocatalysts. Various analytical techniques such as scanning electron microscope (SEM), energy-dispersive X-ray spectroscopy (EDS), photoluminescence (PL) and X-ray diffraction (XRD) were used for the characterization of the novel photocatalysts. It was proven that agrowastes can also enhance the photocatalytic activity of a ZnO-based photocatalyst as pure metals. The combination of MO/GS/A/ZnO/Ag in a 1:1:1 ratio resulted in a lower band gap of 1.59 eV, as compared to the band gap of 2.96 eV for ZnO/Ag. These photocatalysts' efficiency was also tested on the photodegradation of polycyclic aromatic hydrocarbon (PAHs) derived from coal leaching in various water sources such as acidic mine drainage, alkaline mine drainage and sewage wastewater. From MO/GS/A/ZnO/Ag, the removal efficiency was found to be 69.59%, 61.07% and 61.68%, compared to 52.62%, 37.96 and 44.30% using ZnO/Ag in acidic mine drainage, alkaline mine drainage and sewage wastewater for 60 min under solar irradiation.

Keywords: Heterogeneous photocatalyst, Band gap, Acidic mine drainage, Alkaline mine drainage, PAHs

Introduction

Wastewater's impact on the environment is among the main topics studied in recent years due to the continuous release of organic pollutants from various activities such as oil spills, coking processes and gasification (Gaurav et al. 2021). Most of these pollutants end up in various water sources with different physiochemical properties. The pH of these waters can deeply affect the chemistry of the water in the presence of pollutants derived from the aforementioned petroleum-related activities (Zipper et al. 2018). Several studies have been conducted using various metal oxides; however, titanium dioxide (TiO_2) and zinc oxide (ZnO) have been widely used as either semiconductors or nanoparticles in various applications and especially in wastewater treatment (Nguyen et al. 2020; Rani and Shanker 2019).

ZnO has been one of the most exploited metal oxide and n-type semiconductors that have been prioritized due to its multifunctional in various applications (Thema et al. 2015). Metal oxide can further be synthesized by precipitation, hydrolysis, pyrolysis, hydrothermal, electrodeposition, chemical methods and sol–gel processes

*Correspondence: 37465597@student.g.nwu.ac.za

[1] Water Pollution Monitoring and Remediation Initiatives Research Group, Centre of Excellence in Carbon-Based Fuels, North-West University, P. Bag X6001, Potchefstroom 2520, South Africa
Full list of author information is available at the end of the article

(Davar et al. 2015; Pandiyarasan et al. 2014). However, the sol–gel method has been commonly used due to its adaptability, simplicity, reliability and cost-effectiveness (Ganesan et al. 2020; Fan et al. 2020). By synthesizing metal oxides their size and morphology can be influenced by manipulating the pH, varying the annealing temperature, the rate of the reaction, and the additives in the medium to obtain a readily active metal oxide (Davar et al. 2015). The metal oxides can either be synthesised physically, chemically or biologically. However, the physical and chemical methods for synthesizing metal oxide have resulted to be costly and releasing hazards. Therefore, a greener approach has been the most promising method to mitigate these issues since less attention has been given to them (Thovhogi et al. 2015).

Moringa oleifera seed has been used for medicine (Milla et al. 2021) and its application in nanotechnology due to its enrichments in minerals such as calcium, potassium, zinc, magnesium, iron, phosphorous and copper have made it effective in synthesizing a metal oxide (El-Massry et al. 2013; Tovar et al. 2020; Jadhav et al. 2022). Its antioxidants like quercetin and chlorogenic acids such as flavonoids, phenolics, astragalin, anthocyanins, cinnamates, and carotenoids as well as the presence of terpenes, quinines, saponins, alkaloids, proteins, tannins, and vitamin C have a benefit on its uses (Gopalakrishnan et al. 2016). In addition, it has also been proven to be a good reducing agent, capping and stabilizing agent for metals (Aisida et al. 2019).

Cow bones that are predominant in hydroxyapatite (referred to as Apatite) have been used for wastewater treatment (Muretta et al. 2022). The adsorptive properties of bone char derived from cow bones have been tested in various wastewater treatments and proven to be effective (Muretta et al. 2022). The greener application to produce heterogeneous catalysis and its calcium, phosphate, and filler have been made to improve the conventional method (Hart and Aliu 2022). Their contribution to producing high ion exchange, good structural flexibility and also as a good potential renewable source has been suggested to be used in various applications (Iriarte-Velasco et al. 2018).

Groundnut shells have been used for wastewater treatment however, it has been reported that calcinating the groundnut shells can improve the effectiveness of the adsorption capacity (Bedane et al. 2019). Various functional groups such as alkyl, carboxyl, amide, hydroxyl, carbonyl, and alkyne are widely responsible in groundnut shells for the elimination of organic pollutants (Li et al. 2019).

Groundnut shells have been used to synthesize ZnO metal oxide to assist in the photodegradation of organic pollutants (Kamaraj et al. 2021; Dhiman and Sharma 2019; Wu et al. 2019). These agrowastes can be used to synthesize ZnO and therefore improve the ability to produce electrons from their valence bands to the conduction bands while the electrons are excited is indicative of the band gap that has made them useful in a wide range of various applications, especially in wastewater treatment (Selvaraj et al. 2022).

Figure 1 is a schematic representation of the process where the photons, with energy *hv,* are radiated on the material, creating a band gap that is lower than the excitation energy to ensure the delay of the electron recombination.

Conventional methods like coagulation, flocculation, sedimentation, adsorption and membrane processes have been widely used for the removal of organic pollutants from wastewater (Smol and Włodarczyk-Makuła 2017). The limitations of these conventional methods such as production costs and the release of by-products such as carbon dioxide and methane gas have made them less applicable. Photocatalysts have been proven to be the best candidates for the degradation of organic pollutants. Their performance can be further improved by introducing a metal which contributes to a delay of electron recombination holes as well as lowering the band gap to obtain a spontaneous photodegradation (Meenakshi and Sivasamy 2022; Selvaraj et al. 2022).

Since metals have been proven to delay the electron recombination hole and narrow the bandgap, *Moringa oleifera* seed (MO), groundnut shells (GS) and apatite (A) agrowastes have been introduced to replace and enhance the photocatalytic activity of ZnO. Biological methods for synthesizing ZnO metal oxide using MO, GS and A benefit from simplicity, eco-friendliness and extended antimicrobial activity. The presence of metabolites and phytochemicals in MO, GS and A such as terpenoids, alkaloids, flavonoids, proteins, peptides, and tannins increased the biosynthetic manufacturing of ZnO.

Material and methods

In this study, chemicals were purchased from Rochelle Chemicals & Lab Equipment, including zinc acetate dihydrate ($Zn(Ac)_2.2H_2O$, 98%) and silver nitrate ($AgNO_3$, 99.9%). Acidic mine drainage was collected from

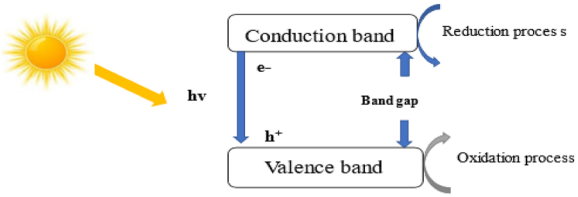

Fig. 1 Schematic representation of the photocatalysis process

Witbank, together with alkaline mine drainage from Middleburg, sewage wastewater from the Cape Town municipality and coal tar from Newcastle in KwaZulu-Natal, all in South Africa.

Synthesis of a zinc oxide semiconductor

A mass of 3 g $Zn(Ac)_2.2H_2O$ was powdered, using a mortar and pestle and it was calcined for 4 h at 350 °C in a furnace with a heating rate of 1 °C/min.

Preparation of ZnO/Ag and MO/GS/A/ZnO/Ag heterogeneous photocatalysts

Biomasses such as *Moringa oleifera* seed, groundnut shells and apatite derived from cow bones were sourced at a nearby market in Cape Town, South Africa. Each biomass was grounded using a grinder to obtain particles at a size of 100 > 150 µm and was washed with deionised water more than 3 times using a centrifuge to remove any impurities. The collected materials were then dried for 24 h at a temperature of 60 °C using an oven.

Heterogeneous photocatalysts were prepared following the sol–gel synthesis with modification (Mukwevho et al. 2020). A mass of 0.2 g of $Zn(C_2H_3O_2)_2\ 2H_2O$ and 0.1 g of Ag were mixed into a volume of 50 mL of deionised water. The solution of ZnO and Ag was stirred to ensure a homogenous mixture and 1 g each of the selected agro-waste MO, GS and A in the ratio (1:1:1) wt.% was added to the mixture. The prepared volume of 2M of NaOH was used to adjust the pH until a pH of 12 was obtained. The overall mixture was stirred at 250 rpm for 2 h. After completing this process, it was centrifuged for 20 min at 6000 rpm whereby the precipitants were obtained, and the material was dried in an oven at a temperature of 80 °C for 24 h.

Procedure for the photocatalyst degradation of PAHs in various water sources using MO/GS/A/ZnO/Ag and ZnO/Ag

A mass of 5 g of coal tar containing a PAH concentration of 2916.47 mg/L was analyzed using the Gas Chromatography Thermo Scientific (TSQ 8000) (Cape Town, South Africa) Triple Quadrupole MS technique.

The prepared MO/GS/A/ZnO/Ag and ZnO/Ag were used for the photodegradation of PAHs in a 5 g of coal tar that was leached into various water sources at a concentration of 1.8125 mg/L in sewage wastewater, 19.2553 mg/L in acidic and 1.6154 mg/L in alkaline mine drainage in a 300 mL leachate for 8 weeks respectively.

The mass of 2.5 g of MO/GS/A/ZnO/Ag or ZnO/Ag (Zhao et al. 2020) was considerable in the leachate of 300 mL under solar irradiation in 20 min, 40 min and 60 min under solar irradiation. Therefore, Eqs. 1–3 are the reactions that may occur during the photodegradation of PAHs in the sewage wastewater, acidic and alkaline mine drainage using MO/GS/ZnO/Ag and ZnO/Ag photocatalysts PAHs in water sources.

$$\text{MO/GS/A/ZnO/Ag or ZnO/Ag} + \text{hv} \rightarrow e^- + h^+ \quad (1)$$

$$O_2 + e^- \rightarrow {}^{\cdot}O_2 - + e^- \quad (2)$$

$$H_2O + h^+ \rightarrow {}^{\cdot}OH + H^+ \quad (3)$$

Although various scavengers are available when adding a catalyst to a reaction, hydroxyl and superoxide are widely recognized as effective oxidizing agents for organic pollutants. However, hydroxyl is produced with or without a catalyst, even in the spilling of water, and it is also highly reactive with organic pollutants (Nguyen et al. 2020). The photodegradation of PAHs is dependent on various parameters such as the physiochemistry of the water (pH, dissolved organic carbon, ionic strength, temperature (Gutierrez-Urbano et al. 2021)), the properties of the photocatalyst (narrow band-gap, delay of the electron recombination hole (Guo et al. 2022)) and solar irradiation (Kaur et al. 2020; Li et al. 2020). Also, the absorption experiment was also conducted in the absence of solar irradiation which is observed in Tables 5, 6, 7 and 8. It was found that the wavelength of 360 nm to 420 nm was responsible for the degradation of various PAHs derived from coal tar.

The photodegradation (%) of PAHs in sewage wastewater, acidic and alkaline mine drainage at room temperature by MO/GS/A/ZnO/Ag or ZnO/Ag was obtained using the Eq. 4.

$$\text{Photodegradation}(\%) = \frac{\text{Initial concentration(Ci)} - \text{Final concentration(Ct)}}{\text{Initial concentration(Ci)}} \times 100 \quad (4)$$

The initial and residual concentrations are given a symbol Ci and Ct that is related to the contact time (t) between the pollutants and the catalyst under solar irradiation.

Results and discussions

Characterisations

UV–Vis absorption spectroscopy

UV–Vis absorption spectrometry (Perkin Elmer UV–Vis lambda 25 spectrometer) was used to determine the optical absorption spectra of the synthesized photocatalysts MO/GS/A/Ag/ZnO to be 376 nm, followed by 269 nm of ZnO/Ag and 339 nm of ZnO respectively The effective of the optical absorption spectrum was to provide the structure of the synthesized material.

The optical band gap value of the synthesized material can be obtained from the optical absorption spectra by extrapolating the straight line of $(h\nu\,\alpha)$ the plot versus the energy $(h\nu)$, based on Eqs. 5–7.

$$\alpha = A\left(h\nu - E_g\right)^n \tag{5}$$

$$(h\nu\,\alpha) = A\left(h\nu - E_g\right)^{1/2} \tag{6}$$

$$\left(E_g\right) = \frac{hc}{\lambda} = \frac{1250}{\lambda} \tag{7}$$

The incorporation of MO/GS/A to synthesize complex heterogeneous photocatalysts (MO/GS/A/ZnO/Ag) resulted in a narrow bandgap and enhanced the absorbance in the visible region as compared to the parent semiconductor (ZnO).

Table 1 The band gaps were obtained for various combinations in the production of a suitable photocatalyst

Photocatalysts	The bandgap (eV)
ZnO/Ag/MO/GS/A	1.59
ZnO/MO/A/GS	1.63
ZnO/A	2.15
ZnO/MO/A	2.49
ZnO/GS	2.51
ZnO/Ag/A	2.59
ZnO/Ag/GS	2.71
ZnO/MO	2.74
ZnO/Ag/MO	2.80
ZnO/MO/GS	2.85
ZnO/Ag	2.96
ZnO	3.35 (Parental)

In this study, various agrowastes were synthesized to produce various heterogeneous photocatalysts shown in Table 1.

The study found that the application of a biological method in combination with various agrowastes for the synthesis of heterogeneous photocatalysts contributed to narrowing the band gap in agreement with literature studies (Yu et al. 2016; Kumar and Luxmi 2021).

By incorporating MO/GS/A agrowastes and Ag metal into ZnO, the absorption spectra of the parental ZnO (376 nm) reduces to MO/GS/A/ZnO/Ag (269 nm) and further to ZnO/Ag (339 nm).

The addition of these agrowastes MO, GS, A and metal such as Ag into ZnO have resulted to reduce the bandgap of the parental ZnO (3.35 eV) to ZnO/MO (2.74 eV), ZnO/GS (2.51 eV), ZnO/A (2.15 eV) and ZnO/Ag (2.96 eV). From these agrowastes it occurs that A agrowastes resulted to narrow the bandgap of ZnO. Beside these agrowastes influence to reduce the bandgap, their impurities also contribute to the narrower of the bandgap (Crowley et al. 2016).

Energy-dispersive X-ray spectroscopy

Energy-dispersive X-ray spectroscopy (EDS) (Nova NanoSEM using an Oxford X-max 20mm^2 detector and INCA software) was used to determine the elemental composition of MO, GS and A presented in Fig. 2. The presence of the oxygen element in these materials and the synthesized ZnO from MO, GS, A and Ag will therefore best explain the delay of the electron recombination holes (Moussawi and Patra 2016). Figure 2e MO/GS/A/ZnO/Ag shows a higher oxygen concentration as compared to ZnO/Ag. In the raw material, the sharp peak in Fig. 2a MO is shown to have a high oxygen content, followed by Fig. 2c A and Fig. 2b GS.

The oxygen content in the raw material and the synthesized material can best be explained as obtaining a delay in the electrons recombination hole and that can be observed in the photoluminescence (PL).

PL spectra

Photoluminescence was used and recorded on a PerkinElmer LS55 Luminescence Spectrometer. The excitation wavelength (λ) of 310 nm for the raw materials (MO, GS and A) and 300 nm for the synthesized materials MO/GS/A/ZnO/Ag, MO/ZnO/Ag, GS/ZnO/Ag, A/ZnO/Ag and (ZnO/Ag) were observed. Figure 4 shows the PL emission spectra for both the raw materials and the synthesized materials at room temperature.

As observed in Fig. 3a MO provided a broader shoulder sharp peak with a higher PL intensity followed by GS and

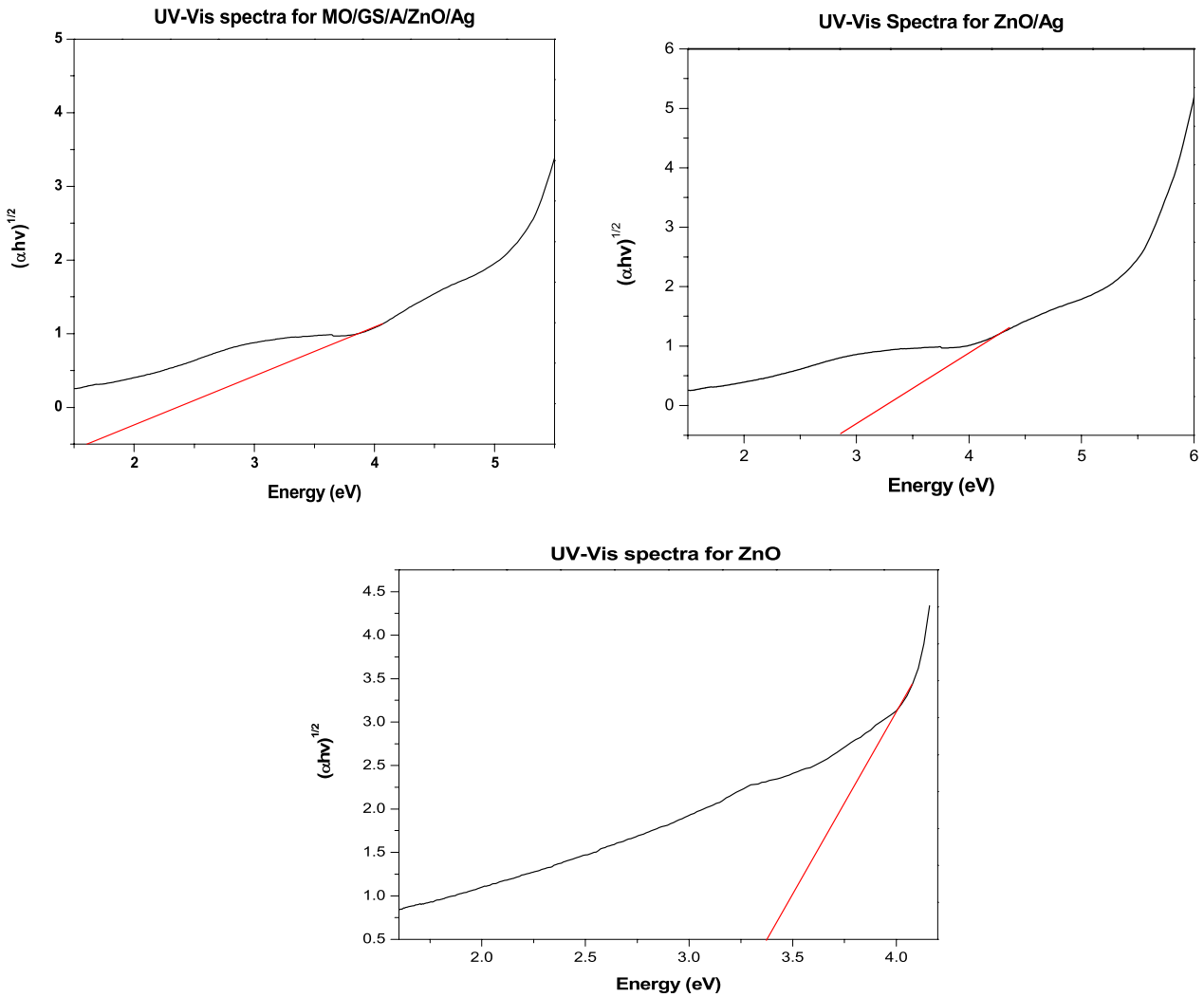

Fig. 2 Optical absorption spectra of the synthesized samples MO/GS/A/ZnO/AG, ZnO/Ag and ZnO

A. The following synthesized materials MO/ZnO/Ag, GS/ZnO/Ag and A/ZnO/Ag indicated that the presence of A provided a lower PL intensity, followed by GS and MO which resulted in a higher photoactivity. According to Ji et al. (2020), the doping of metals was found to reduce the PL intensity and increase the photocatalytic activity, as shown in Fig. 4: MO/GS/A/ZnO/Ag as compared to ZnO/Ag. The incorporation of agrowastes combined resulted in a decrease in PL intensity (Komaraiah et al. 2019).

It also shows that a higher oxygen content in MO/GS/A/ZnO/Ag is also responsible to influence the electron recombination. This also causes a delay in the recombination of the electrons (Park et al. 2003). This mostly occurs when the electrons are in contact with the material and the oxygen in that material happens to trap the produced electrons from the visible light (solar irradiation) (He et al. 2019).

Scanning electron microscope

A scanning electron microscope NovaNano SEM and the Tescan MIRA3 RISE SEM was used to determine the structure and the morphology of the material presented in Fig. 5. MO showed the plant cells that constituted fairy pores and GS showed the fibres (stems), whereas A shows a smooth structure derived from lipid compounds known as phospholipids. The image of the heterogeneous photocatalyst MO/GS/A/ZnO/Ag shows tissue cells (stem plant) and ZnO/Ag shows nanocrystals.

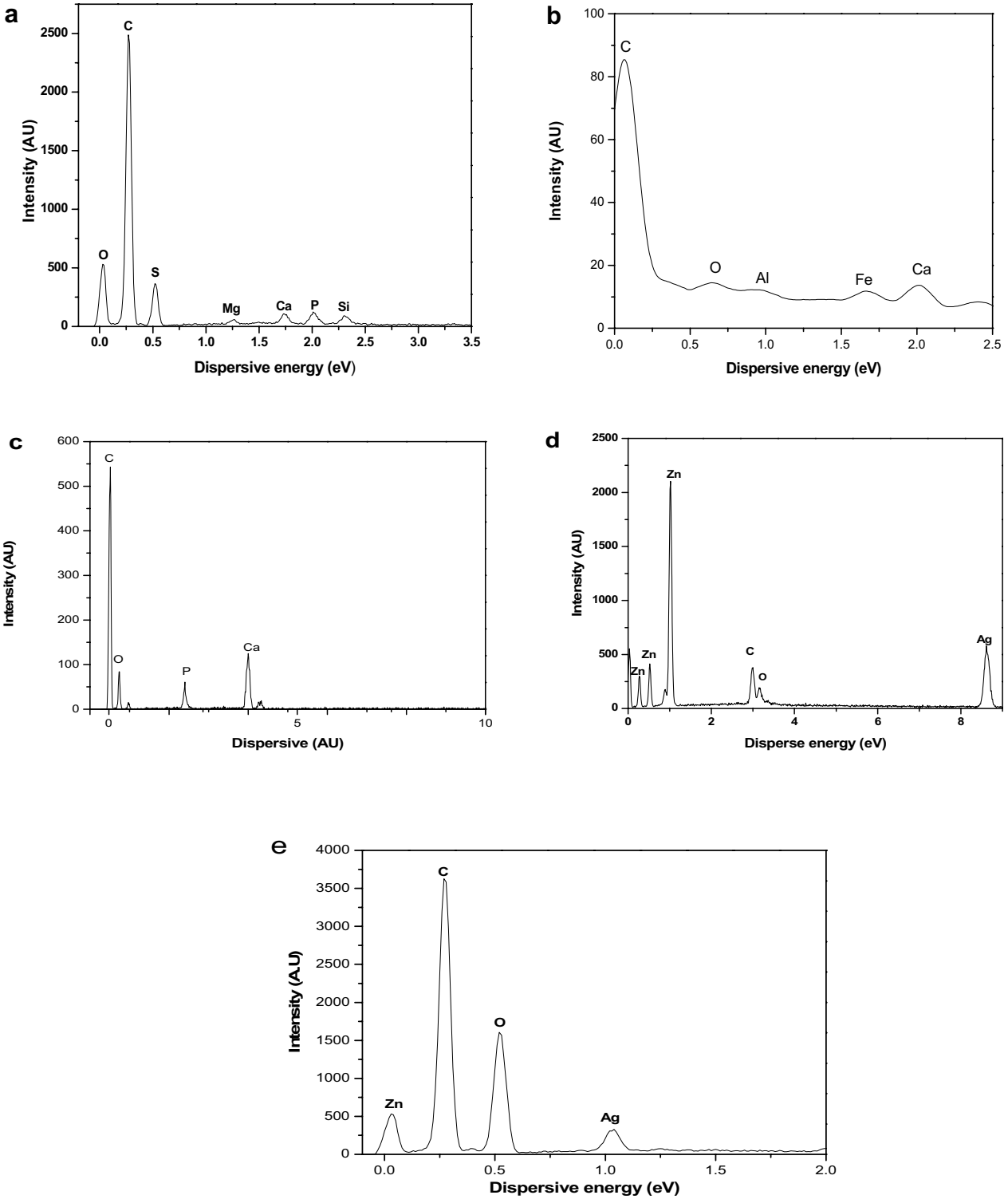

Fig. 3 EDS patterns for the raw material: **a** MO; **b** GS; **c** A and for the synthesized material; **d** ZnO/Ag; **e** MO/GS/A/ZnO/Ag

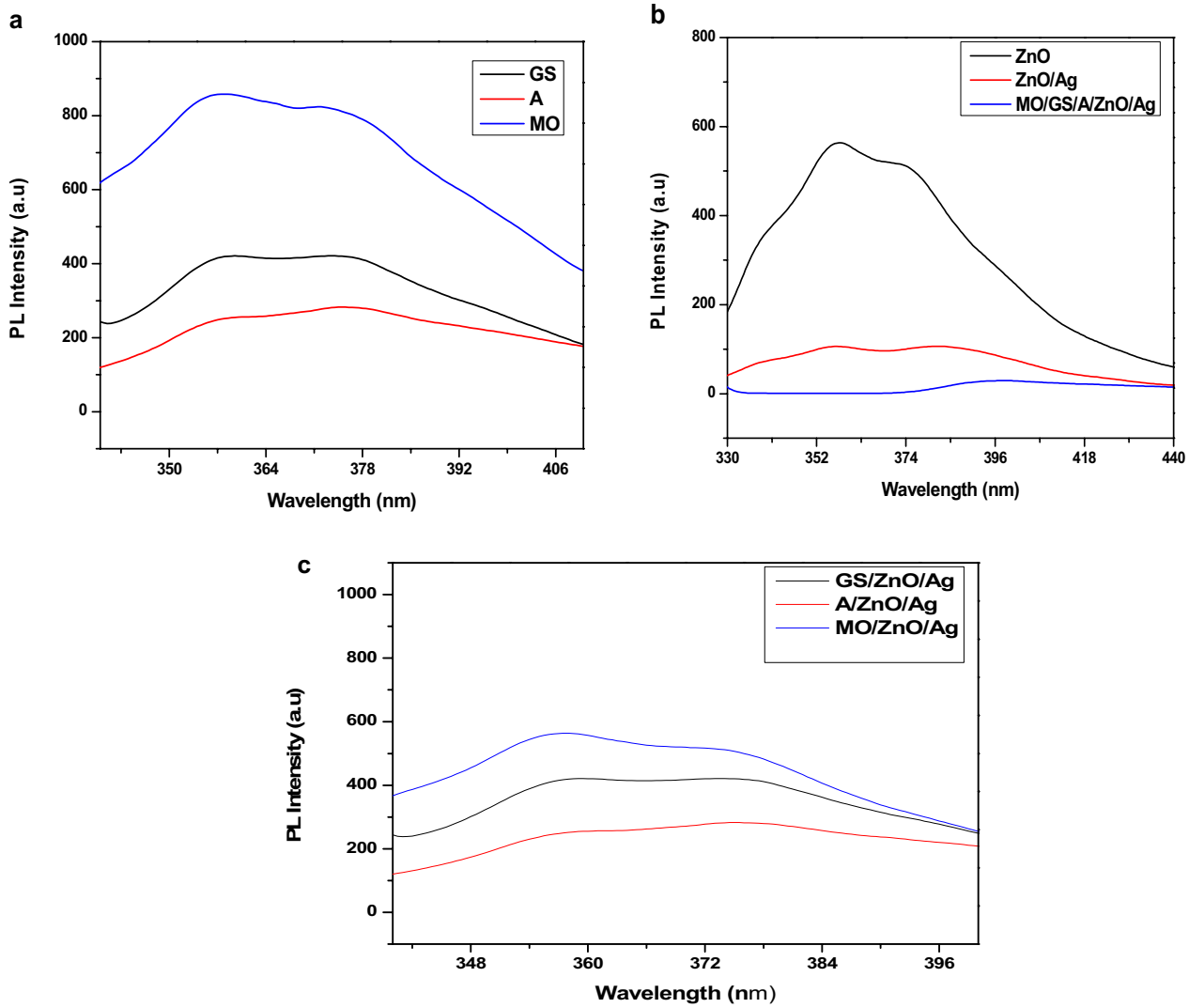

Fig. 4 Optical properties of the MO/GS/A/ZnO/Ag, MO/ZnO/Ag, GS/ZnO/Ag, A/ZnO/Ag heterogeneous photocatalyst and ZnO/Ag photocatalyst (**a**) PL of raw materials, **b**, **c** are PL of the synthesized material

X-ray diffraction

X-ray diffraction (XRD) Powder XRD measurements were recorded on an Analytical XPERT-PRO diffractometer, using Ni filtered CuKα radiation (λ = 1.5406 Å) at 45 kV/40 mA which was used to determine the crystal structure of the materials. The diffraction measurements in Fig. 6 were collected at room temperature in a Bragg–Brentano geometry. The XRD of MO/GS/A/ZnO/Ag and ZnO/Ag did not completely corroborate with the hexagonal structure of the raw reference pattern: ZnO, 00-036-1451 and Ag, 00-004-0783. Since the studied ZnO and Ag were used in combination with the biomasses, the impurities could have interfered with or influenced the diffraction peak. The sharp diffraction peaks were observed at 2θ values 32, 33, 36, 48, 56, 57, 63 and 68 degrees. These peaks are indexed as (100), (002), (101), (102), (110), (103) and (112), and diffraction lattice planes respectively which confirm the hexagonal wurtzite structure for the synthesized materials (MO/GS/A/ZnO/A and ZnO/Ag).

The elemental composition of the various biomasses used in the synthesis of photocatalysts using ICP-MS

In this study, the elementary analysis of the metal content in MO, GS and A using Thermo ICap6300 ICP-AES is represented in Table 2.

This study agrees with Yu et al. (2016) have reported, the doping of various elements narrowed the band gap.

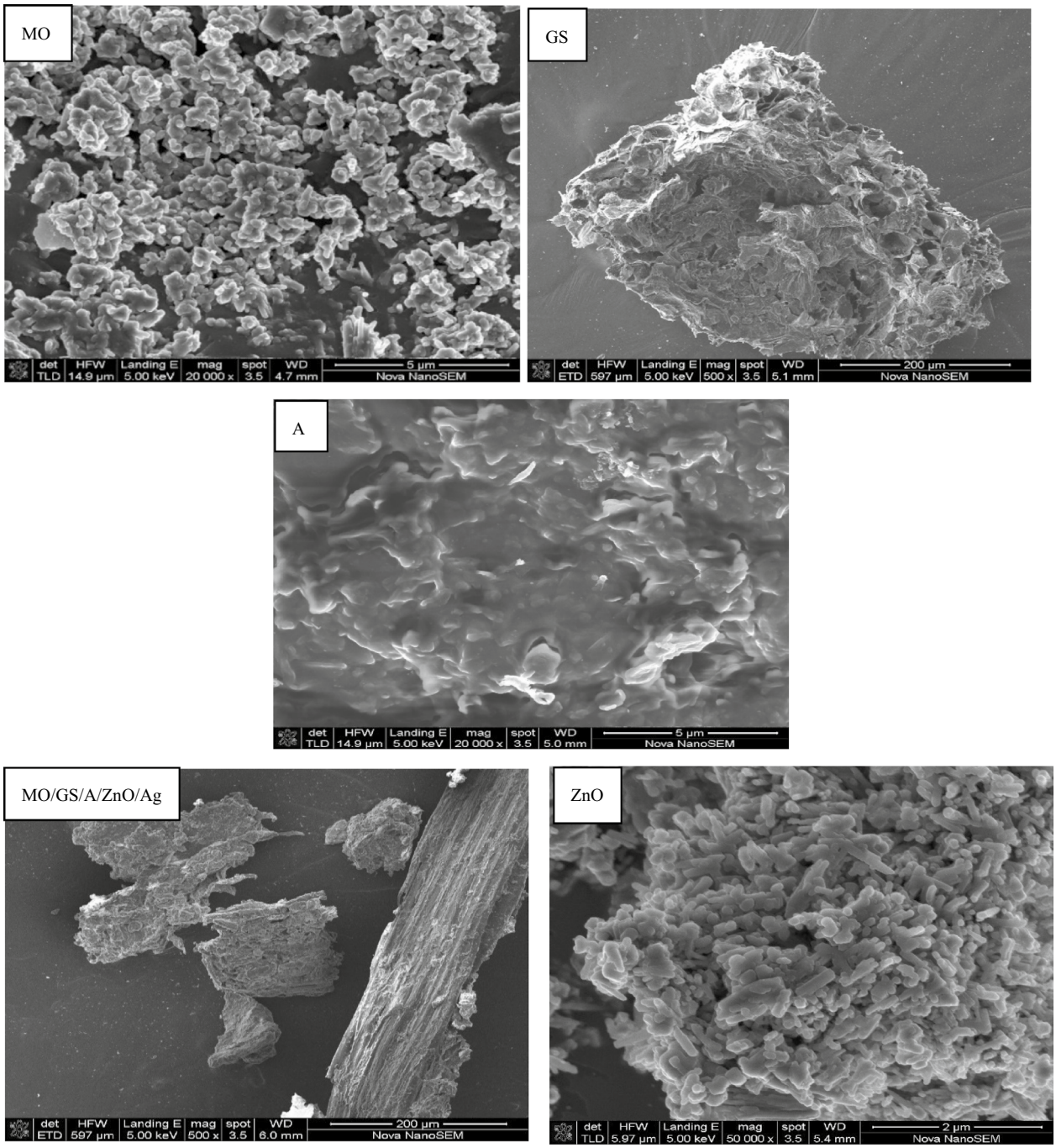

Fig. 5 SEM images of the raw materials (MO, GS and A) and synthesized materials (MO/GS/A/ZnO/Ag and ZnO/Ag)

Fu et al. (2018) have reported, earth metals are effective as compared to noble metals to enhance photocatalytic activity. Various studies (Selvaraj et al. 2022; Boruah et al. 2019; Uma et al. 2022; Naciri et al. 2020) have proven that the dopant of strontium (Sr) which is a rare earth metal, happens to have a high photocatalytic activity which can be determined under the visible spectrum (Márquez-Herrera et al. 2016). In this study, Sr was highly concentrated in apatite followed by groundnut shells and *Moringa oleifera*. Due to the presence of Sr in apatite, it can confirmed that apatite can provide a higher photocatalytic as compared to

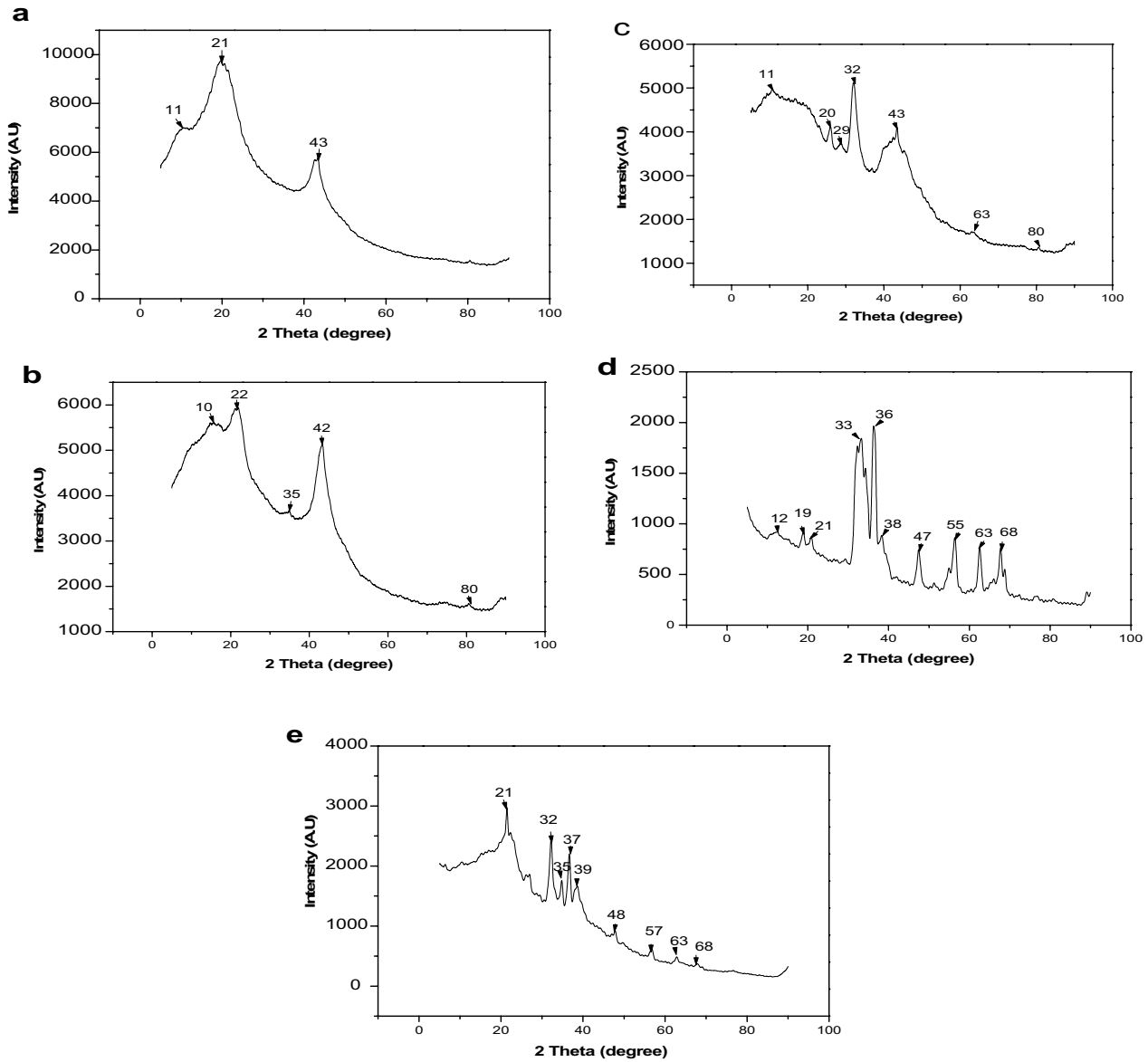

Fig. 6 XRD spectra of raw material **a** MO; **b** GS; **c** A and synthesized material **d** MO/GS/A/ZnO/Ag; **e** ZnO/Ag

MO and GS. In addition, the remaining metal content in these agrowastes also contributed to enhancing the photocatalytic activity of the parental ZnO (Rani and Shanker 2019; Jana et al. 2015) (Table 3).

Photodegradation of PAHs in various water sources

The decomposition of PAHs in coal tar using Gas Chromatography–Mass Spectrometry (GC–MS) with a Thermo Scientific (TSQ 8000) (Cape Town, South Africa) Triple Quadrupole MS is illustrated in Table 4. Naphthalene, phenanthrene, fluoranthene, acenaphthylene and fluorene are the most concentrated PAHs in coal tar at 788 mg/L, 632 mg/L, 395 mg/L and 356 mg/L. From Tables 5, 6 and 7, the photodegradation of PAHs in acidic mine drainage, alkaline mine drainage and sewage wastewater are presented and their removal efficiency are illustrated in Table 8.

From Tables 5, 6 and 7, the photodegradation of PAHs was most favoured in acidic mine drainage followed by sewage wastewater and alkaline mine drainage under solar irradiation over time. This was succeeded according to the physiochemistry of sewage wastewater and alkaline mine drainage that influenced the photodegradation

Table 2 Raw material elementary analysis using ICP-MS

Elements	Apatite	Groundnut shells	*Moringa oleifera* seed
Rare metals (ug/kg)			
Boron (B)	4886	14,040	3345
Aluminium (Al)	286,978	1,379,257	335,251
Vanadium (V)	857	2464	972
Chromium (Cr)	47,821	5375	13,577
Manganese (Mn)	29,085	49,766	13,797
Iron (Fe)	3,305,754	1,626,773	624,167
Cobalt (Co)	749	491	179
Nickel (Ni)	12,202	2585	2437
Copper (Cu)	14,339	9104	10,354
Zinc (Zn)	112,006	81,561	54,864
Arsenic (As)	612	249	79
Selenium (Se)	71	50	801
Strontium (Sr)	387,273	31,469	22,730
Molybdenum (Mo)	579	261	269
Cadmium (Cd)	67	30	54
Tin (Sn)	3083	593	232
Antimony (Sb)	125	21	19
Barium (Ba)	61,927	51,511	11,780
Mercury (Hg)	13	13	10
Lead (Pb)	6433	1479	947
Metals (mg/g)			
Sodium (Na)	4,435,644	80,587	30,317
Magnesium (Mg)	3,245,487	1,414,007	1,352,569
Silicon (Si)	115,349	302,102	398,638
Phosphorous (P)	108,054,240	1,083,471	7,167,605
Potassium (K)	343,351	2,654,548	777,148
Calcium (Ca)	221,203,248	4,871,463	3,061,091
Non-metals (%)			
Nitrogen (N)	3.72	1.11	4.36
Carbon (C)	20.01	44.58	54.18
Hydrogen (H)	4.41	8.59	10.41
Sulphur (S)	1.65	2.93	2.36

Table 4 Concentration of PAHs concentration in coal tar at room temperature

PAHs (pollutants)	Concentration (mg/L)
NAP	788
ACY	356
ACE	18
FL	327
PHE	632
ANT	245
FLU	395
PYR	266
BaA	91
CHY	126
BbF	75
Blkf	71
BaP	92
DahA	56
IP	8
Bghip	21

of PAHs (Batchamen Mougnol et al. 2022). The molecular weight PAH of 2 to 3 rings such as naphthalene, anthracene and phenanthrene degraded rapidly from their normal regions over time due to their volatility which able them to be destabilized.

The introduction of MO, GS and A were due to their abundance, availability and eco-friendly. Their ability to narrow the band gap and delay the electron recombination charger carrier highly contributes successfully to photocatalytic degradation. The higher oxygen content in the material happen to traps the electrons and prevents them from recombining (Biroju and Giri 2017). The presence of O_2 in the material in water with an OH- happens to form Hydrogen peroxide (H_2O_2). Therefore, the radical that was responsible for degrading the PAHs derived from coal tar was H_2O_2.

Table 3 The elemental composition of the various biomasses used in the synthesis of photocatalysts as determined by EDS analysis

MO (wt%)	C	O	Mg	Si	P	S	Ca
	69.75	28.33	0.22	0.19	0.57	0.68	0.27
GS (wt%)	C	O	Ca				
	54.06	44.84	1.10				
A (wt%)	C	O	P	Ca			
	49.19	30.04	6.20	14.52			
MO/GS/A/ZnO/Ag (wt%)	C	O	Zn	Ag			
	53.03	36.25	3.65	7.06			
ZnO/Ag (wt%)	C	O	Zn	Ag			
	23.08	19.32	34.00	23.60			

Table 5 Photodegradation of PAHs in acidic mine drainage

PAHs	Initial concentration	Catalyst	20 min Dark	40 min Dark	60 min Dark	20 min Solar	40 min Solar	60 min Solar	Catalyst	20 min Dark	40 min Dark	60 min Dark	20 min Solar	40 min Solar	60 min Solar
NAP	0.0031	MO/GS/A/ZnO/Ag	0.0023	0.0020	0.0017	0.0014	0.0011	0.0012	ZnO/Ag	0.0030	0.0028	0.0026	0.0015	0.0013	0.0013
ACY	0.1302		0.1296	0.1283	0.1277	0.0967	0.1068	0.0931		0.1300	0.1298	0.1286	0.1105	0.0097	0.1001
ACE	0		0	0	0	0	0	0		0	0	0	0	0	0
FL	0		0	0	0	0	0	0		0	0	0	0	0	0
PHE	0.0181		0.0163	0.0158	0.0152	0.0067	0.0063	0.0057		0.0177	0.0173	0.0164	0.0072	0.0084	0.0070
ANT	18.9847		17.0934	16.9862	16.730	5.8110	5.7913	5.7010		18.6046	18.5927	18.5864	9.0047	9.1091	8.9122
FLU	0.0020		0.0017	0.0016	0.0017	0.0015	0.0012	0.0011		0.0019	0.0018	0.0018	0.0016	0.0015	0.0015
PYR	0		0	0	0	0	0	0		0	0	0	0	0	0
BaA	0.1114		0.1093	0.1091	0.1087	0.0503	0.0510	0.0496		0.1101	0.1091	0.1089	0.1018	0.0981	0.0974
CHY	0.0012		0.0010	0.0009	0.0010	0.0008	0.0001	0.0001		0.0011	0.0010	0.0009	0.0009	0.0002	0.0002
BbF	0		0	0	0	0	0	0		0	0	0	0	0	0
Blkf	0		0	0	0	0	0	0		0	0	0	0	0	0
BaP	0.0046		0.0038	0.0036	0.0034	0.0037	0.0026	0.0023		0.0042	0.0040	0.0040	0.0039	0.0030	0.0031
DahA	0		0	0	0	0	0	0		0	0	0	0	0	0
IP	0		0	0	0	0	0	0		0	0	0	0	0	0
Bghip	0		0	0	0	0	0	0		0	0	0	0	0	0
PAHs photo-degradation	19.2553		17.3574	17.2475	16.9894	5.9856	5.9604	5.8540		18.8726	18.8585	18.8496	9.2321	9.2313	9.1228

Table 6 Photodegradation of PAHs in alkaline mine drainage

PAHs	Initial concentration	Catalyst	20 min Dark	40 min Dark	60 min Dark	20 min Solar	40 min Solar	60 min Solar	Catalyst	20 min Dark	40 min Dark	60 min Dark	20 min Solar	40 min Solar	60 min Solar
NAP	0.7615	MO/GS/A/ZnO/Ag	0.7528	0.7518	0.7511	0.5005	0.5013	0.3780	ZnO/Ag	0.7547	0.7545	0.7540	0.5253	0.5102	0.4955
ACY	0.2596		0.2437	0.2414	0.2403	0.0419	0.0291	0.0210		0.2509	0.2501	0.2449	0.1974	0.0976	0.1003
ACE	0.0020		0.0016	0.0017	0.0017	0.0010	0.0001	0.0001		0.0018	0.0018	0.0016	0.0014	0.0012	0.0012
FL	0.0030		0.0019	0.0018	0.0019	0.0009	0.0010	0.0009		0.0026	0.0025	0.0022	0.0019	0.0012	0.0011
PHE	0.0447		0.0438	0.0427	0.0416	0.0297	0.0270	0.0261		0.0445	0.0443	0.0439	0.0371	0.0318	0.0211
ANT	0.5388		0.5157	0.4974	0.4831	0.2119	0.2005	0.2004		0.5208	0.5193	0.5037	0.4724	0.3816	0.3799
FLU	0.0039		0.0028	0.0027	0.0027	0.0021	0.0016	0.0011		0.0032	0.0031	0.0029	0.0026	0.0025	0.0017
PYR	0.0019		0.0016	0.0015	0.0015	0.0013	0.0012	0.0012		0.0018	0.0017	0.0017	0.0017	0.0016	0.0014
BaA	0		0	0	0	0	0	0		0	0	0	0	0	0
CHY	0		0	0	0	0	0	0		0	0	0	0	0	0
BbF	0		0	0	0	0	0	0		0	0	0	0	0	0
Blkf	0		0	0	0	0	0	0		0	0	0	0	0	0
BaP	0		0	0	0	0	0	0		0	0	0	0	0	0
DahA	0		0	0	0	0	0	0		0	0	0	0	0	0
IP	0		0	0	0	0	0	0		0	0	0	0	0	0
Bghip	0		0	0	0	0	0	0		0	0	0	0	0	0
PAHs photo-degradation	1.6154		1.5639	15.410	1.5239	0.7893	0.7618	0.6288		1.5803	1.5773	1.5549	1.2398	1.0277	1.0022

Table 7 Photodegradation of PAHs sewage wastewater

PAHs	Initial concentration	Catalyst	20 min Dark	40 min Dark	60 min Dark	20 min Solar	40 min Solar	60 min Solar	Catalyst	20 min Dark	40 min Dark	60 min Dark	20 min Solar	40 min Solar	60 min Solar
NAP	0.0069	MO/GS/A/ZnO/Ag	0.0062	0.0061	0.0060	0.0045	0.0041	0.0032	ZnO/Ag	0.0068	0.0067	0.0063	0.0051	0.0051	0.0044
ACY	0.0489		0.0427	0.0414	0.0412	0.0308	0.0261	0.0247		0.0439	0.0421	0.0417	0.0391	0.0265	0.0271
ACE	0		0	0	0	0	0	0		0	0	0	0	0	0
FL	0.009		0.0085	0.0084	0.0084	0.0043	0.0042	0.0009		0.0087	0.0081	0.0081	0.0050	0.0049	0.0045
PHE	0.0961		0.0938	0.0925	0.0912	0.0223	0.0219	0.0193		0.0944	0.0939	0.0931	0.0767	0.0743	0.0731
ANT	0.1758		0.1715	0.1703	0.1709	0.1202	0.1125	0.1083		0.1726	0.1710	0.1699	0.1411	0.113	0.0976
FLU	0.1706		0.1648	0.1645	0.1630	0.1052	0.1015	0.1004		0.1690	0.1685	0.1679	0.1491	0.1205	0.1073
PYR	0.1389		0.1360	0.1348	0.1334	0.0119	0.0110	0.0109		0.1380	0.1377	0.1368	0.1196	0.1174	0.0843
BaA	0.1888		0.1687	0.1684	0.1683	0.1329	0.1171	0.1066		0.1718	0.1710	0.1709	0.1046	0.1021	0.0981
CHY	0.1170		0.1152	0.1152	0.1141	0.0716	0.0673	0.0642		0.1167	0.1156	0.1148	0.1002	0.0901	0.0860
BbF	0.2216		0.2152	0.2150	0.2149	0.1222	0.1217	0.0898		0.2187	0.2184	0.2181	0.1929	0.1001	0.1001
Blkf	0.1563		0.1528	0.1524	0.1517	0.0593	0.0875	0.0981		0.1559	0.1557	0.1553	0.1052	0.0909	0.0998
BaP	0.2185		0.2009	0.2006	0.2005	0.1005	0.1001	0.0193		0.2017	0.2016	0.2008	0.1852	0.1087	0.1005
DahA	0.1278		0.1267	0.1261	0.1253	0.0110	0.0101	0.0095		0.1275	0.1272	0.1268	0.1108	0.0897	0.0655
IP	0.0345		0.0327	0.0323	0.0317	0.0051	0.0037	0.0038		0.0335	0.0332	0.0329	0.0195	0.0162	0.0171
Bghip	0.1018		0.1012	0.1011	0.1010	0.0530	0.0429	0.0275		0.1016	0.1014	0.1012	0.0824	0.0487	0.0441
PAHs photo-degradation	1.8125		1.7364	1.7291	1.5307	0.8548	0.8317	0.6946		1.7608	1.7521	1.7446	1.3465	1.0965	1.0095

Table 8 Removal efficiency of PAHs in contact time

Water sources	Removal efficiency (%) MO/GS/A/ZnO/Ag						Removal efficiency (%) ZnO/Ag					
	20 min Dark	40 min Dark	60 min Dark	20 min Solar	40 min Solar	60 min Solar	20 min Dark	40 min Dark	60 min Dark	20 min Solar	40 min Solar	60 min Solar
Acidic mine drainage	9.86	10.43	11.78	68.91	69.05	69.59	1.99	2.06	2.11	52.05	52.06	52.62
Alkaline mine drainage	3.19	4.61	5.66	51.14	52.84	61.07	2.17	2.36	3.74	23.25	36.38	37.96
Sewage wastewater	4.20	4.60	15.55	52.84	54.11	61.68	2.85	3.33	3.75	25.71	39.50	44.30

The modification of the material MO/GS/A/ZnO/Ag was found to provide a low PL intensity which contributed to poorer recombination rates of photo-induced charge carriers as compared to ZnO/Ag (Nagajyothi et al. 2020; Mukwevho et al. 2020; Park et al. 2003). The removal efficiency was better in acidic mine drainage, followed by alkaline mine drainage and sewage wastewater over time under solar irradiation.

Various studies (Sescu et al. 2020; Wang et al. 2021; Haruna et al. 2020; Sanakousar et al. 2022) have confirmed that, doping of metals can potentially enhance the photocatalytic process by achieving a spontaneous photodegradation outcome. Therefore, the content of the metal in these agrowastes was proven to contribute to the photodegradation of PAHs in various water sources.

In this study, the introduction of these MO, GS, and A indicate their ability to produce electrons and trapped them from their valance bands to their conduction bands which will further favour the photodegradation.

The effectiveness of adsorption in a dark was also proven to be effective however the removal efficiency was lesser as compared to using solar irradiation. It was observed that the higher removal efficiency in 60 min was obtained on the sewage wastewater, acidic and alkaline mine drainage using MO/GS/A/ZnOAg while using ZnO/Ag, the higher removal efficiency was obtained in sewage, alkaline and acidic mine drainage.

A study conducted by Tong et al. (2015) reported that the narrow band gap of a photocatalyst resulted in the rapid recombination of electrons and holes which restricted the photocatalytic efficiency. However, this study had contrary findings, in agreement with Guo et al. (2022), that MO/GS/A/ZnO/ZnO provided a delay in the recombination of electron hole-pairs and narrow band gap. Its application in the photodegradation of PAHs in different water sources under solar irradiation drastically improved over time. The application of this heterogeneous photocatalyst generated high photons, also by being able to produce reactive scavengers in comparison to ZnO/Ag. In this study, it was found that agrowastes that contain various metals (including Sr which is reported to have high photocatalytic activity and can be naturally found in a few agrowastes) obtained a higher removal efficiency than metals without agrowastes.

Conclusion

The application of agrowastes was found to be a better candidate as compared to metals in obtaining a higher removal efficiency. The synthesis of complex heterogeneous photocatalysts resulted in narrowing the band gap and its oxygen content resulted in retarding the electron recombination. Free energy in the form of solar irradiation was effective in destabilizing the aromatic ring in PAHs in water sources. In the study hydrogen peroxide was the radical responsible for destabilizing the aromatic rings from the PAHs. Since PAHs were highly concentrated in acidic mine drainage depending on the water physiochemistry like the pH and total organic carbon. Time was also observed to be an important factor in obtaining acceptable photodegradation in various water sources. The heterogeneous photocatalyst MO/GS/A/ZnO/Ag was found to be effective as compared to ZnO/Ag. Their application in wastewater treatment was tested and proven that MO/GS/A/ZnO/Ag was highly effective under solar irradiation, with a removal efficiency of 69.59%, 61.07% and 61.68% as compared to ZnO/Ag with the removal efficiency of 52.62%, 37.96%, and 44.30%. The adsorption of PAHs was also tested in a dark chamber and again MO/GS/A/ZnO/Ag happen to be favoured in comparison to ZnO/Ag. The metals content in MO, GS and A were proven to have a significant outcome on the photocatalytic activity and photodegradation. The abundance, availability, cost-effectiveness, oxygen and metal contents of these agrowastes have made them to be favoured in the study.

Acknowledgements

The authors are thankful to the sponsors, the Water Research Commission (WRC, Project 2974) and the North-West University in South Africa.

Author contributions

JBBM—Conceptualization, data curation, format analysis, investigation, methodology, sofware, validation, visualization, writing original draft. FW—funding acquisition, methodology, supervision; project administration, resources, supervision, writing—review and editing. EF-K—Methodology, project administration; supervision; writing—review and editing. ARAA—Supervision, methodology, writing—review and editing. SKON—Supervision,

methodology, writing—review and editing. All authors read and approved the final manuscript.

Funding
Open access funding provided by North West University. Water Research Commission (WRC, Project 2974) and the North-West University in South Africa.

Availability of data and materials
Not applicable.

Declarations

Ethics approval and consent to participate
Not applicable.

Consent for publication
Not applicable.

Competing interests
The authors declare no conflict of interest.

Author details
[1]Water Pollution Monitoring and Remediation Initiatives Research Group, Centre of Excellence in Carbon-Based Fuels, North-West University, P. Bag X6001, Potchefstroom 2520, South Africa. [2]Department of Mining Engineering, College of Science Engineering and Technology, University of South Africa, Florida Science Campus, Roodepoort, South Africa. [3]DEWA R&D Centre, Dubai Electricity and Water Authority (DEWA), Dubai, United Arab Emirates.

Received: 18 July 2022 Accepted: 8 November 2022
Published online: 20 November 2022

References

Aisida SO, Ugwoke E, Uwais A, Iroegbu C, Botha S, Ahmad I, Maaza M, Ezema FI (2019) Incubation period induced biogenic synthesis of PEG enhanced *Moringa oleifera* silver nanocapsules and its antibacterial activity. J Polym Res 26:1–11

Batchamen Mougnol JB, Waanders F, Fosso-Kankeu E, Al Alili AR (2022) Leaching of polycyclic aromatic hydrocarbons from the coal tar in sewage wastewater, acidic and alkaline mine drainage. Int J Environ Res Public Health 19:4791

Bedane AH, Guo TX, Eić M, Xiao H (2019) Adsorption of volatile organic compounds on peanut shell activated carbon. Can J Chem Eng 97:238–246

Biroju RK, Giri P (2017) Strong visible and near infrared photoluminescence from ZnO nanorods/nanowires grown on single layer graphene studied using sub-band gap excitation. J Appl Phys 122:044302

Boruah B, Gupta R, Modak JM, Madras G (2019) Enhanced photocatalysis and bacterial inhibition in Nb 2 O 5 via versatile doping with metals (Sr, Y, Zr, and Ag): a critical assessment. Nanoscale Adv 1:2748–2760

Crowley JM, Tahir-Kheli J, Goddard WA III (2016) Resolution of the band gap prediction problem for materials design. J Phys Chem Lett 7:1198–1203

Davar F, Majedi A, Mirzaei A (2015) Green synthesis of ZnO nanoparticles and its application in the degradation of some dyes. J Am Ceram Soc 98:1739–1746

Dhiman N, Sharma N (2019) Batch adsorption studies on the removal of ciprofloxacin hydrochloride from aqueous solution using ZnO nanoparticles and groundnut (*Arachis hypogaea*) shell powder: a comparison. Indian Chem Eng 61:67–76

El-Massry FH, Mossa ME, Youssef SM (2013) *Moringa oleifera* plant. Egypt J Agric Res 91:1597–1909

Fan Q, Li D, Li J, Wang C (2020) Structure and piezoelectricity properties of V-doped ZnO thin films fabricated by sol-gel method. J Alloy Compd 829:154483

Fu J, Kyzas GZ, Cai Z, Deliyanni EA, Liu W, Zhao D (2018) Photocatalytic degradation of phenanthrene by graphite oxide-TiO2-Sr (OH) 2/SrCO3 nanocomposite under solar irradiation: effects of water quality parameters and predictive modeling. Chem Eng J 335:290–300

Ganesan V, Hariram M, Vivekanandhan S, Muthuramkumar S (2020) *Periconium* sp. (endophytic fungi) extract mediated sol-gel synthesis of ZnO nanoparticles for antimicrobial and antioxidant applications. Mater Sci Semicond Process 105:104739

Gaurav GK, Mehmood T, Kumar M, Cheng L, Sathishkumar K, Kumar A, Yadav D (2021) Review on polycyclic aromatic hydrocarbons (PAHs) migration from wastewater. J Contam Hydrol 236:103715

Gopalakrishnan L, Doriya K, Kumar DS (2016) *Moringa oleifera*: a review on nutritive importance and its medicinal application. Food Sci Human Wellness 5:49–56

Guo L, Xu F, Liu Z, Zhang M, Ma D, Lai C, Liu S, Li L, Fu Y, Qin L (2022) Constructing benzene ring modified graphitic carbon nitride with narrowed bandgap and enhanced molecular oxygen activation for efficient photocatalytic degradation of oxytetracycline. Sep Purif Technol 294:121170

Gutierrez-Urbano I, Villen-Guzman M, Perez-Recuerda R, Rodriguez-Maroto JM (2021) Removal of polycyclic aromatic hydrocarbons (PAHs) in conventional drinking water treatment processes. J Contam Hydrol 243:103888

Hart A, Aliu E (2022) Materials from eggshells and animal bones and their catalytic applications. Design Appl Hydroxyapatite Based Catalysts. 437–479

Haruna A, Abdulkadir I, Idris S (2020) Photocatalytic activity and doping effects of BiFeO3 nanoparticles in model organic dyes. Heliyon 6:e03237

He J, Fang W-H, Long R (2019) Unravelling the effects of oxidation state of interstitial iodine and oxygen passivation on charge trapping and recombination in CH 3 NH 3 PbI 3 perovskite: a time-domain ab initio study. Chem Sci 10:10079–10088

Iriarte-Velasco U, Ayastuy JL, Boukha Z, Bravo R, Gutierrez-Ortiz MÁ (2018) Transition metals supported on bone-derived hydroxyapatite as potential catalysts for the Water-Gas Shift reaction. Renew Energy 115:641–648

Jadhav V. Bhagare A, Ali IH, Dhayagude S, Lokhande D, Aher J, Jameel M, Dutta M (2022) Role of *Moringa oleifera* on green synthesis of metal/metal oxide nanomaterials. J Nanomater 2022

Jana S, Garain S, Sen S, Mandal D (2015) The influence of hydrogen bonding on the dielectric constant and the piezoelectric energy harvesting performance of hydrated metal salt mediated PVDF films. Phys Chem Chem Phys 17:17429–17436

Ji S, Yuan X, Cao S, Ji W, Zhang H, Wang Y, Li H, Zhao J, Zou B (2020) Near-unity red Mn2+ photoluminescence quantum yield of doped CsPbCl3 nanocrystals with Cd incorporation. J Phys Chem Lett 11:2142–2149

Kamaraj P, Sridharan M, Arockiaselvi J, Pushpamalini T, Vivekanand P (2021) Low cost synthesis of ZnO nanoparticles and evaluation of their photocatalytic activity. Mater Today 36:873–877

Kaur K, Badru R, Singh PP, Kaushal S (2020) Photodegradation of organic pollutants using heterojunctions: a review. J Environ Chem Eng 8:103666

Komaraiah D, Radha E, Kalarikkal N, Sivakumar J, Reddy MR, Sayanna R (2019) Structural, optical and photoluminescence studies of sol-gel synthesized pure and iron doped TiO2 photocatalysts. Ceram Int 45:25060–25068

Kumar A, Luxmi V (2021) Development of an efficient eco-friendly photocatalyst using agro-waste turmeric leaves and its characterizations. Optik 242:167057

Li L, Zou D, Xiao Z, Zeng X, Zhang L, Jiang L, Wang A, Ge D, Zhang G, Liu F (2019) Biochar as a sorbent for emerging contaminants enables improvements in waste management and sustainable resource use. J Clean Prod 210:1324–1342

Li Y, Shen Q, Guan R, Xue J, Liu X, Jia H, Xu B, Wu Y (2020) AC@ TiO 2 yolk–shell heterostructure for synchronous photothermal–photocatalytic degradation of organic pollutants. J Mater Chem C 8:1025–1040

Márquez-Herrera A, Ovando-Medina VM, Castillo-Reyes BE, Zapata-Torres M, Meléndez-Lira M, González-Castañeda J (2016) Facile synthesis of SrCO3-Sr (OH) 2/PPy nanocomposite with enhanced photocatalytic activity under visible light. Materials 9:30

Meenakshi G, Sivasamy A (2022) Enhanced photocatalytic activities of CeO2@ ZnO core-shell nanostar particles through delayed electron hole recombination process. Colloids Surf, A 645:128920

Milla PG, Peñalver R, Nieto G (2021) Health benefits of uses and applications of *Moringa oleifera* in bakery products. Plants 10:318

Moussawi RN, Patra D (2016) Nanoparticle self-assembled grain like curcumin conjugated ZnO: curcumin conjugation enhances removal of perylene, fluoranthene and chrysene by ZnO. Sci Rep 6:1–13

Mukwevho N, Gusain R, Fosso-Kankeu E, Kumar N, Waanders F, Ray SS (2020) Removal of naphthalene from simulated wastewater through

adsorption-photodegradation by ZnO/Ag/GO nanocomposite. J Ind Eng Chem 81:393–404
Muretta JE, Prieto-Centurion D, LaDouceur R, Kirtley JD (2022) Unique chemistry and structure of pyrolyzed bovine bone for enhanced aqueous metals adsorption. Waste Biomass Valorization**.** 1–20.
Naciri Y, Hsini A, Ajmal Z, Bouddouch A, Bakiz B, Navío J, Albourine A, Valmalette J, Ezahri M, Benlhachemi A (2020) Influence of Sr-doping on structural, optical and photocatalytic properties of synthesized Ca3 (PO4) 2. J Colloid Interface Sci 572:269–280
Nagajyothi PC, Prabhakar Vattikuti SV, Devarayapalli KC, Yoo K, Shim J, Sreekanth TVM (2020) Green synthesis: photocatalytic degradation of textile dyes using metal and metal oxide nanoparticles-latest trends and advancements. Crit Rev Environ Sci Technol 50:2617–2723
Nguyen V-H, Thi L-AP, Van Le Q, Singh P, Raizada P, Kajitvichyanukul P (2020) Tailored photocatalysts and revealed reaction pathways for photodegradation of polycyclic aromatic hydrocarbons (PAHs) in water, soil and other sources. Chemosphere 260:127529
Pandiyarasan V, Shanmugapriya P, Thanuja M, Anusuya T, Vairavaraja P (2014) Synthesis and characterization of ZnO nanoparticles—a green chemistry approach. Asian J of Adv Basic Sci 3:94–101
Park W, Jun Y, Jung S, Yi G-C (2003) Excitonic emissions observed in ZnO single crystal nanorods. Appl Phys Lett 82:964–966
Rani M, Shanker U (2019) Sunlight mediated improved photocatalytic degradation of carcinogenic benz [a] anthracene and benzo [a] pyrene by zinc oxide encapsulated hexacyanoferrate nanocomposite. J Photochem Photobiol, A 381:111861
Sanakousar F, Vidyasagar C, Jiménez-Pérez V, Prakash K (2022) Recent progress on visible-light-driven metal and non-metal doped ZnO nanostructures for photocatalytic degradation of organic pollutants. Mater Sci Semicond Process 140:106390
Selvaraj S, Palanivel B, Patrick S, Krishna Mohan M, Navaneethan M, Ponnusamy S, Muthamizhchelvan C (2022) Effect of Sr doping in ZnO microspheres for solar light-driven photodegradation of organic pollutants. J Mater Sci: Mater Electron 33:8777–8788
Sescu AM, Favier L, Lutic D, Soto-Donoso N, Ciobanu G, Harja M (2020) TiO2 doped with noble metals as an efficient solution for the photodegradation of hazardous organic water pollutants at ambient conditions. Water 13:19
Smol M, Włodarczyk-Makuła M (2017) The effectiveness in the removal of PAHs from aqueous solutions in physical and chemical processes: a review. Polycyclic Aromat Compd 37:292–313
Thema F, Manikandan E, Dhlamini M, Maaza M (2015) Green synthesis of ZnO nanoparticles via *Agathosma betulina* natural extract. Mater Lett 161:124–127
Thovhogi N, Diallo A, Gurib-Fakim A, Maaza M (2015) Nanoparticles green synthesis by *Hibiscus sabdariffa* flower extract: main physical properties. J Alloy Compd 647:392–396
Tong Z, Yang D, Xiao T, Tian Y, Jiang Z (2015) Biomimetic fabrication of g-C3N4/TiO2 nanosheets with enhanced photocatalytic activity toward organic pollutant degradation. Chem Eng J 260:117–125
Tovar GI, Briceño S, Suarez J, Flores S, González G (2020) Biogenic synthesis of iron oxide nanoparticles using *Moringa oleifera* and chitosan and its evaluation on corn germination. Environ Nanotechnol Monit Manag 14:100350
Uma HB, Kumar MSV, Ananda S (2022) Semiconductor-assisted photodegradation of textile dye, photo-voltaic and antibacterial property of electrochemically synthesized Sr-doped CuO nano photocatalysts. J Mol Struct 1264:133110
Wang Y, Liu X, Guo L, Shang L, Ge S, Song G, Naik N, Shao Q, Lin J, Guo Z (2021) Metal organic framework-derived C-doped ZnO/TiO2 nanocomposite catalysts for enhanced photodegradation of Rhodamine B. J Colloid Interface Sci 599:566–576
Wu H, Chen R, Du H, Zhang J, Shi L, Qin Y, Yue L, Wang J (2019) Synthesis of activated carbon from peanut shell as dye adsorbents for wastewater treatment. Adsorpt Sci Technol 37:34–48
Yu W, Zhang J, Peng T (2016) New insight into the enhanced photocatalytic activity of N-, C-and S-doped ZnO photocatalysts. Appl Catal B 181:220–227
Zhao Z, Omer AA, Qin Z, Osman S, Xia L, Singh RP (2020) Cu/N-codoped TiO2 prepared by the sol-gel method for phenanthrene removal under visible light irradiation. Environ Sci Pollut Res 27:17530–17540
Zipper CE, Skousen JG, Jage CR (2018) Passive treatment of acid-mine drainage.

Publisher's Note